Electronic Structure and Excited State Dynamics of the NIR-II Emissive Molybdenum(III) Analog to the Molecular Ruby

Winald R. Kitzmann[1,2], David Hunger[4], Antti-Pekka M. Reponen[2], Christoph Förster[1], Roland Schoch[3], Matthias Bauer[3], Sascha Feldmann[2], Joris van Slageren[4], Katja Heinze[1,*]

[1] *Department of Chemistry, Johannes Gutenberg-University of Mainz, Duesbergweg 10–14, 55128 Mainz, Germany. E-Mail: Katja.Heinze@uni-mainz.de*

[2] *Rowland Institute, Harvard University, 100 Edwin H. Land Boulevard, Cambridge, MA-02142, USA.*

[3] *Faculty of Science, Chemistry Department and Centre for Sustainable Systems Design, Paderborn University, 33098 Paderborn, Germany.*

[4] *Institute of Physical Chemistry and Center for, Integrated Quantum Science and Technology, University of Stuttgart, Pfaffenwaldring 55, 70569 Stuttgart, Germany.*

Keywords: Excited states, molybdenum, electron paramagnetic resonance spectroscopy, spin-flip, zero-field splitting, ultrafast spectroscopy.

Abstract

Photoactive chromium(III) complexes saw a conceptual breakthrough with the discovery of the prototypical molecular ruby, *mer*-$[Cr(ddpd)_2]^{3+}$ (ddpd = *N*,*N*'-dimethyl-*N*,*N*'-dipyridin-2-ylpyridine-2,6-diamine), that shows intense long-lived near-infrared (NIR) phosphorescence from metal-centered spin-flip states. In contrast to the numerous studies on chromium(III) photophysics, only ten luminescent molybdenum(III) complexes have been reported so far. Here, we present the synthesis and characterization of *mer*-MoX_3(ddpd) (**1**: X = Cl, **2**: X = Br) and *cisfac*-$[Mo(ddpd)_2]^{3+}$ (*cisfac*-$\mathbf{[3]^{3+}}$), an isomeric heavy homolog of the prototypical molecular ruby. For *cisfac*-$\mathbf{[3]^{3+}}$, we found strong zero-field splitting using magnetic susceptibility measurements and electron paramagnetic resonance (EPR) spectroscopy. Electronic spectra covering the spin-forbidden transitions show that the spin-flip states in *mer*-**1**, *mer*-**2** and *cisfac*-$\mathbf{[3]^{3+}}$ are much lower in energy than in comparable chromium(III) compounds. While all three complexes show weak spin-flip phosphorescence in the NIR-II, the emission of *cisfac*-$\mathbf{[3]^{3+}}$ peaking at 1550 nm is particularly low in energy. Femtosecond-transient absorption spectroscopy reveals a short excited state lifetime of 1.4 ns, six orders of magnitude shorter than that of *mer*-$[Cr(ddpd)_2]^{3+}$. Using density functional theory and *ab initio* multi-reference calculations, we break down the reasons for this disparity, and derive principles for the design of future stable photoactive molybdenum(III) complexes.

Introduction

Research in the field of photochemistry and photophysics of transition metal complexes in the past few decades primarily focused on materials based on precious metals due to their favorable excited state properties.[1–5] In the past 10 years, scientific curiosity drove researchers to explore

earth-abundant metal complexes in more detail.[6–11] These efforts uncovered photoactive complexes with intriguing excited state properties that can show unique reactivity following novel mechanisms.[12–22]

In particular, photoactive chromium(III) complexes saw a renaissance.[23,24] It was kicked off by the discovery of design principles that allowed access to materials with bright long-lived excited states. The seed for this revolution was the so-called molecular ruby, *mer*-$[Cr(ddpd)_2]^{3+}$ (ddpd = *N*,*N*'-dimethyl-*N*,*N*'-dipyridin-2-ylpyridine-2,6-diamine), that shows a dual phosphorescence in the near-infrared (NIR) with a high quantum yield and lifetime of 13.7 % and 1.12 ms, respectively.[25,26] The emission originates from nested metal-centered doublet states that only differ from the quartet ground state by a flipped spin (spin-flip emission). In the molecular ruby, the ligand ddpd produces a large ligand field splitting that shifts distorted $^4T_2$ states to higher energy which would otherwise enable non-radiative deactivation of the emissive spin-flip states.[14,27]

Because no antibonding orbitals are occupied in the spin-flip states, they only show negligible excited state distortion and hence sharp emission bands.[24] The energy of these nested excited states depends on the interelectronic repulsion which is determined by the nephelauxetic effect, *i.e.* the extent of delocalization of the d-electrons on the ligands, which is often expressed using the Racah parameters *B* and *C* from ligand field theory.[24,28] Covalent M–L bonds lead to low-energy spin-flip states while ionic bonds increase the excited state energy. Phosphorescence from chromium(III) complexes is usually found between 720 and 800 nm.[24] Recently, it was shown that the emission energy can be tuned from the red (709 nm)[29] to NIR-II spectral region (up to 1067 nm) by ligand design.[30–32]

An important deactivation pathway for low-energy luminescence is energy transfer to vibrational overtones of the ligand or the solvent.[33] Statistic deuteration of ddpd boosted the luminescence quantum yield of *mer*-$[Cr(ddpd)_2]^{3+}$ to 30 %.[34] Overall, complexes with spin-flip excited states have been applied in optical sensing of hydrostatic pressure, temperature and oxygen partial pressure,[35,36] as energy and electron transfer catalysts,[15,37,38] as sensitizers for photon upconversion,[22,39] as qubits[40–43] and for circularly polarized luminescence.[44–48]

Generally, spin-flip emission is neither limited to chromium(III) nor the d^3 electron configuration.[24] Other metal-centers such as vanadium(III) or manganese(IV) have been explored as well and show dramatically different excited state energies due to their different M–L bond covalency.[19,49–52]

In contrast to the large body of work covering octahedral chromium(III) complexes,[23,53–57] those of the heavier homolog molybdenum(III) have remained largely unexplored.[24] Although both ions share the same d^3 electron configuration, molybdenum(III) complexes are more labile and prone to oxidation and dimerization due to the higher ionic radius of the central metal.[58,59] Homoleptic Mo^{III} complexes are particularly rare with most of the reported examples being stabilized by halides.[59–63]

Recent reports on mononuclear molybdenum(III) complexes include the investigation of the strongly solvatochromic $[Mo(bpy)Cl_4]^-$[64] (bpy = 2,2'-bipyridine) and the redox chemistry of $[Mo(^{Me}PDP)_2]^{n-}$ (*n* = 0, 1, 2, 3) with a tridentate pyridinepyrrolate ligand ($H_2{}^{Me}PDP$ = 2,6-bis(5-methyl-3-phenyl-1*H*-pyrrol-2-yl)pyridine).[62] Detailed investigations of the zero-field splitting (ZFS) of mononuclear molybdenum complexes are limited to few reports.[65–68] Studies of luminescent molybdenum(III) complexes are equally rare, with only 10 examples covered in

three publications, all of which feature at least three (pseudo)halide ligands.[24,69–72] Due to the low interelectronic repulsion in the extended 4d orbitals, the reported emission is red-shifted compared to typical chromium(III) complexes and located >1100 nm.[24,73] A trend which is also expected when considering the Racah parameter *B* of the free ions (Cr^{3+}: 918 cm^{-1}, Mo^{3+}: 610 cm^{-1}).[73] Hence, molybdenum(III) complexes provide an ideal chemical platform to explore the effects of strong spin-orbit coupling[74] and low interelectronic repulsion on spin-flip states. Additionally, their investigation can provide molecular materials of earth-abundant metals with highly desired luminescence in the NIR-II spectral region without the need to rely on rare-earth elements.[75,76]

Here, we present the synthesis and structural characterization of the heteroleptic halido complexes *mer*-MoX_3(ddpd) (X = Cl: *mer*-**1**, X=Br: *mer*-**2**) and the homoleptic complex *cisfac*-$[Mo(ddpd)_2]^{3+}$ (*cisfac*-**[3]$^{3+}$**). We report their electronic absorption spectra including spin-forbidden absorptions in the red to NIR spectral region. All three complexes show weak spin-flip phosphorescence in the NIR-II in solution at room temperature, with *cisfac*-**[3]$^{3+}$** featuring the lowest spin-flip phosphorescence energy reported to date (λ_{max} = 1550 nm). For *cisfac*-**[3]$^{3+}$**, we also provide a detailed investigation of the ground state electronic structure by means of superconducting quantum interface device (SQUID) magnetometry and EPR spectroscopy, and the excited state dynamics by fs-transient absorption (TA) spectroscopy. We support our experimental results with density functional theory (DFT) and *ab initio* multi-reference quantum chemical calculations.[77]

Results and Discussion

Syntheses and crystal structures

Mer-**1** and *mer*-**2** were obtained from a THF substitution reaction of the precursor complexes *mer*-$MoCl_3(THF)_3$ **I** and *mer*-$MoBr_3(THF)_3$ **II** with the ligand ddpd (Scheme 1).[78–80] The synthesis of the homoleptic complex *cisfac*-**[3]$^{3+}$** as $[BF_4]^-$ and $[PF_6]^-$ salts generally proceeded by treating *mer*-**1** or *mer*-**2** with ddpd in the presence of a halide abstracting agent such as silver(I) or thallium(I) salts under inert conditions (Scheme 1). Composition and purity of the complexes were confirmed using IR spectroscopy, mass spectrometry and elemental analysis (see Supporting Information, SI, Figure S1–Figure S9).

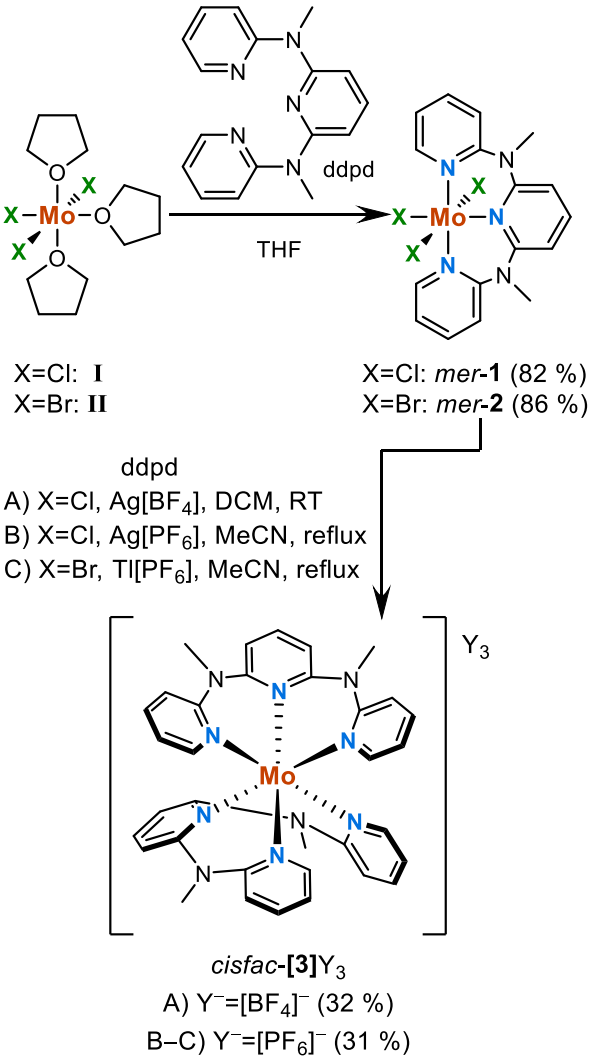

Scheme 1: Synthesis of *mer*-**1**, *mer*-**2** and *cisfac*-**[3]**$^{3+}$ from the precursors **I** and **II**, and the ligand ddpd. Y^- = counterion of **[3]**$^{3+}$, RT = room temperature.

While the meridional configuration of **I** and **II** was preserved in the synthesis of **1** and **2**, **[3]**$^{3+}$ was exclusively isolated with a cis-facial coordination of the ligands regardless of whether the synthesis was performed at room temperature (Route A) or at 82°C (Routes B and C, Scheme 1). This contrasts a previous report on $[V(ddpd)_2]^{2+}$ where the *cisfac*-isomer was obtained as the kinetic and the *mer*-isomer the thermodynamic product at 22 and 82 °C, respectively.[81] Similarly, $[Co(ddpd)_2]^{2+}$ could be isolated as *cisfac*- and *mer*-isomers by rapid and slow crystallization, respectively.[82,83] DFT calculations on **[3]**$^{3+}$ suggest only a slight stabilization of the *mer*-isomer (*ca.* –0.1 eV) with respect to the *cisfac*- and *transfac*-isomers which are placed at almost the same energy (Figure S35). It is possible that a mixture of isomers forms during the halide substitution reactions. Yet only the *cisfac*-isomer readily crystallizes enabling its isolation.

One attempt to synthesize **[3]**$^{3+}$ from *mer*-**2** with $Ag[PF_6]$ as halide abstraction agent produced the binuclear molybdenum(V) complex $[Mo_2(ddpd)_2O_2(\mu\text{-}O)_2][PF_6]_2$ (**[4]**$[PF_6]_2$). Similarly, refluxing $MoCl_3$ with ddpd in MeCN yielded crystals of $Mo_2Cl_2(ddpd)O_2(\mu\text{-}O)_2$ (**5**) and the Lindqvist hexamolybdate[84] $[Hddpd]_2[Mo_6O_{19}]$ ($[Hddpd]_2$**[6]**) with the protonated ddpd ligand serving as a counterion. These results underline the sensitivity of Mo^{III} complexes towards hydrolysis and oxidation that is absent in most Cr^{III} complexes.[24,25]

Single crystals of *mer*-**1**, *mer*-**2**, *cisfac*-**[3]**$^{3+}$ as $[BF_4]^-$ and $[PF_6]^-$ salts, **[4]**$[PF_6]_2$·DCM, **5** and $[Hddpd]_2$**[6]** for X-ray diffraction (XRD) analysis were obtained by slow diffusion of diethyl ether or THF into MeCN or DMSO solutions (Figure 1). *Mer*-**1** and *mer*-**2** crystallize isostructurally in the monoclinic space group $P2_1/n$ (Figure 1, Table S1, Table S4) which has also been reported for the corresponding chromium(III) homologs.[85,86] The crystal structure of *cisfac*-**[3]**$^{3+}$ is strongly influenced by the counterions and cocrystallized solvent molecules (Figure 1, Table S2), similar to the pseudo-polymorphs found for $[Cr(ddpd)_2]^{3+}$.[26] Yet, the geometry of the complex cation *cisfac*-**[3]**$^{3+}$ is mostly unperturbed by the second coordination sphere in the crystal lattice (Table S5).

The average Mo–N and Mo–X (X = Cl, Br) distances observed in the single crystals of *mer*-**1**, *mer*-**2** and *cisfac*-**[3]**$^{3+}$ match those obtained by extended X-ray absorption fine structure spectroscopy at the Mo K-edge of the powders (EXAFS, Figure S11–Figure S15, Table S9–Table S11) and are well reproduced by a structural model derived from DFT calculations (B3LYP/D3BJ/ZORA/TZVP/CPCM(MeCN), Table S4, Table S5).

The symmetric and asymmetric molybdenum(V) dimers **[4]**$[PF_6]_2$·DCM and **5** crystallize in the space groups $C2/c$ and $Pna2_1$, respectively, with facial coordination of the ddpd ligands (Figure 1, Table S3, Table S6, Table S7). The $[Mo_2O_2(\mu\text{-}O)_2]^{2+}$ motif is common for $Mo^V_2O_4L_n$ complexes[87,88] and the short Mo^V–Mo^V distances of *ca.* 2.5 Å are characteristic for Mo–Mo single bonds (Table S6, Table S7).[89] The molybdate(VI) $[Hddpd]_2$**[6]** crystallizes in the space group $C2/c$ and the averaged Mo–O bond lengths in the cluster anion (Figure 1, Table S3, Table S8) conform to previous literature reports.[90]

Overall, the results of our syntheses demonstrate that *mer*-**1**, *mer*-**2** and *cisfac*-**[3]**$^{3+}$ are susceptible to oxidation and hydrolysis in solution, which has also been observed for other molybdenum(III) complexes in previous reports.[58] In the solid state, the three complexes can be handled under air.

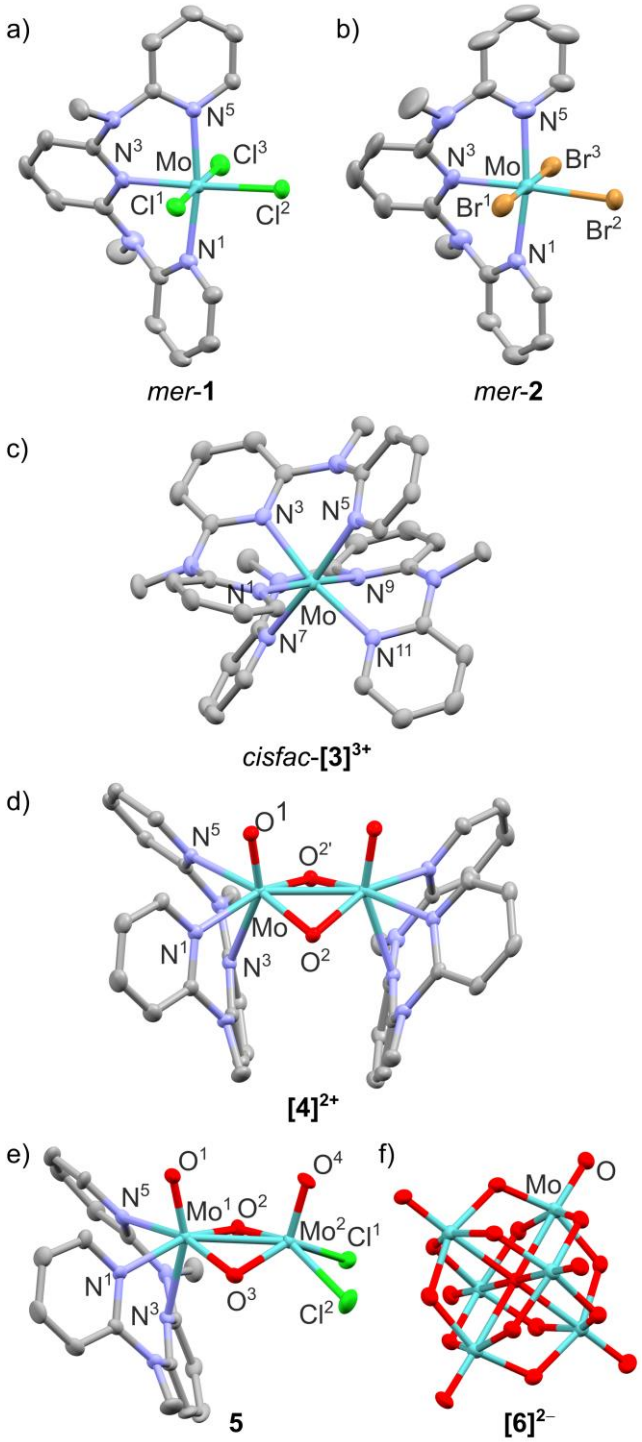

Figure 1: Molecular structures of a) *mer*-**1**, b) *mer*-**2**, c) *cisfac*-$[\mathbf{3}]^{3+}$, d) $[\mathbf{4}]^{2+}$, e) **5** and f) $[\mathbf{6}]^{2-}$. Thermal ellipsoids at 50 % probability. Hydrogen atoms and counterions omitted for clarity. Color code: Grey = carbon, purple = nitrogen, blue = molybdenum, green = chlorine, orange = bromine, red = oxygen. Atom numbering for $[\mathbf{6}]^{2-}$ in Figure S10.

Electronic Structure of the Ground State of *cisfac*-$[\mathbf{3}]^{3+}$

To probe the electronic structure of the ground state in *cisfac*-$[\mathbf{3}]^{3+}$, we performed cyclic voltammetry in solution, high-field (HF) and X-band electron paramagnetic resonance (EPR) spectroscopy, as well as SQUID magnetometry of powders or pressed pellets.

Cisfac-**[3]**$^{3+}$ shows two irreversible oxidation waves at +1.47 and +1.71 V vs. FcH/FcH$^+$ in MeCN (Figure S17, Figure S18, Table 1). On the reductive side, we found three waves with decreasing reversibility (–0.94, –1.76, –2.02 V *vs.* FcH/FcH$^+$). For the assignment of the other oxidation and reduction waves, we optimized the geometries of the respective oxidized and reduced complex and generated their spin densities (Figure S36, Table S13). Based on this analysis, we assign the first wave at –0.94 V *vs.* FcH/FcH$^+$ to a metal-centered reduction ($Mo^{III/II}$). It is plausible that the larger Mo^{III} center is easier to reduce than Cr^{III} in *mer*-[Cr(ddpd)$_2$]$^{3+}$ (–1.11 V *vs.* FcH/FcH$^+$).[25] The second reduction wave in *cisfac*-**[3]**$^{3+}$ at –1.76 V *vs.* FcH/FcH$^+$ can be assigned to a metal-centered reduction ($Mo^{II/I}$). We tentatively assign the wave at –2.02 V *vs.* FcH/FcH$^+$ to a ligand-centered reduction (ddpd/[ddpd]$^{\bullet-}$, Table 1) based on the fact that the reduction of the ligand was found to be irreversible in the free ligand and all ddpd complexes reported so far.[27] The irreversible waves in *cisfac*-**[3]**$^{3+}$ at +1.47 and +1.71 V *vs.* FcH/FcH$^+$ correspond to a metal-centered ($Mo^{IV/III}$) and ligand-centered oxidation ([ddpd]$^{\bullet+}$/ddpd), respectively, according to the DFT calculations (Figure S36, Table S13).

Table 1: Electrochemical data of *cisfac*-**[3]**$^{3+}$ (this work) and *mer*-[Cr(ddpd)$_2$]$^{3+}$[25] with assignments of the redox processes.

cisfac-**[3]**$^{3+}$	*mer*-[Cr(ddpd)$_2$]$^{3+}$
–2.02* (ddpd/[ddpd]$^{\bullet-}$)^a	
–1.76 ($Mo^{II/I}$)^b	–1.94* (ddpd/[ddpd]$^{\bullet-}$)
–0.94 ($Mo^{III/II}$)^b	–1.11 ($Cr^{III/II}$)
+1.47* ($Mo^{IV/III}$)^b	+1.71*
+1.71* ([ddpd]$^{\bullet+}$/ddpd)^b	

All potentials measured in MeCN (0.1 M [^{n}Bu$_4$N][PF$_6$]) and given *vs.* FcH/FcH$^+$. * Irreversible wave. *a* Tentative assignment. *b* Assignment drawn from DFT calculations (Figure S36, Table S13).

To probe the properties of the electronic ground state of *cisfac*-**[3]**$^{3+}$, we first performed SQUID magnetometry on a pressed pellet of the complex from 1.8 to 300 K (Figure 2). The experimental temperature-susceptibility value (χT) is 1.67 cm^3 K mol^{-1} at room temperature and yields a *g*-value of 1.89 based on the Curie law for a $S = {}^3/_2$ spin system.[91] A *g*-value below 2 is expected for less than half-filled d-shells. Additionally, the drop of χT below 50 K hints towards substantial ZFS or an intermolecular exchange pathway in *cisfac*-**[3]**$^{3+}$. The experimental data are reproduced well by spin Hamiltonian simulations using Eq. 1, with the Bohr magneton μ_B, the spin operators $\hat{\boldsymbol{S}}$, $\hat{S}_x$, $\hat{S}_y$, and $\hat{S}_z$, the g-tensor $\boldsymbol{g}$, the magnetic field vector $\boldsymbol{B}$, and the axial and transversal ZFS parameters *D* and *E* (Table 2).[92]

$$\mathcal{H} = \mu_B \hat{\boldsymbol{S}} \cdot \boldsymbol{g} \cdot \boldsymbol{B} + D\hat{S}_z^2 + E\left(\hat{S}_x^2 - \hat{S}_y^2\right) \qquad (1)$$

Table 2: Spin Hamiltonian parameters of *cisfac*-**[3]**[BF$_4$]$_3$ determined by different methods with total electron spin *S*, axial and transversal ZFS parameters *D* and *E*, principal values of the *g*-tensor $g_{xx,yy,zz}$ and exchange coupling constant *J*.

	SQUID^a	HFEPR^a	X-band EPR^b	CASSCF^c
S	3/2	3/2	3/2	3/2
D / cm^{-1}	8.0(1)	6.7(1)	6.7^d	–6.6
E / cm^{-1}	0.8(4)	0.8(5)	0.8^d	1.65
g_{xx}	1.61(1)	1.61(3)	1.61^d	
g_{yy}	2.12(2)	2.12(5)	2.12^d	
g_{zz}	1.90(2)	1.90(3)	1.90^d	

J	–0.7

a Measured in pressed pellet. *b* Measured with a powder sample. Simulated using Eq. S1. *c* SOC-CASSCF(7,12)-NEVPT2. *d* Values taken from HFEPR spectra.

A simulation of the experimental χT curve is possible with D = 8.0(1) cm^{-1}, E = 0.8(4) cm^{-1} and principal values of the g-tensor $g_{xx,yy,zz}$ = [1.61(1), 2.12(2), 1.90(2)]. This set of parameters also reproduced field dependent magnetization curves at temperatures of 1.8, 5, 10 and 20 K (inset in Figure 2). Similar to a previous report on molybdenum(III) complexes, the observed g-values lie below 2.[65]

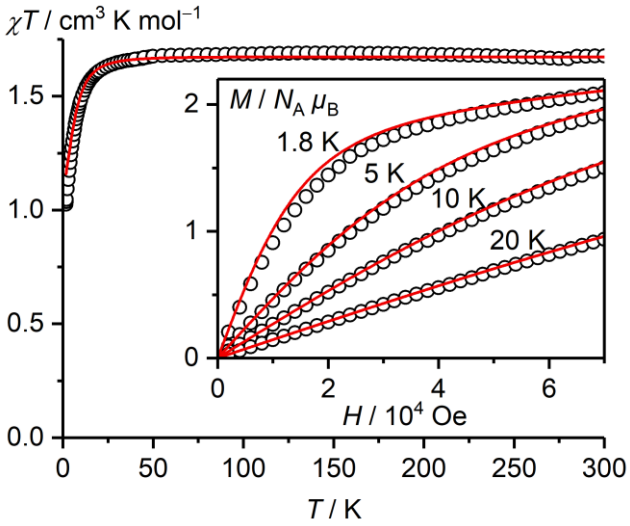

Figure 2: Temperature dependence of χT of *cisfac*-**[3]**$^{3+}$ in a pressed pellet obtained from SQUID magnetometry. Inset: Magnetization M *vs.* magnetic field H at the indicated temperatures. Experimental data is shown as black circles, while simulations based on Eq. 1 with the spin Hamiltonian parameters in Table 2 are shown as red lines.

To complement the magnetometry results, we performed HFEPR spectroscopy[68] between 180–420 GHz at 5 K on the same pellet of *cisfac*-**[3]**$^{3+}$ (Figure 3a). The HFEPR spectra at 5 K show three main features. At 320 GHz, these signals are located at 1.4 T (A, broad), 3.4 T (B, sharp) and 10 T (C, broad) and can be assigned to transitions from $m_S = -1/2$ to $-3/2$ formally forbidden transitions inside the $m_S = \pm 3/2$ doublet in x/y direction, and the Kramers doublet $m_S = -1/2$ to $+1/2$, respectively (see SI for details). Hence, the ZFS parameter D = 6.7 cm^{-1} and an approximate value for E of 0.83 cm^{-1} can be extracted from signals A and B, respectively. These values agree well with spin Hamiltonian simulations (Eq. 1) of the HFEPR spectra, which yield D = 6.7(1) cm^{-1}, E = 0.8(5) cm^{-1} and $g_{xx,yy,zz}$ = [1.61(3), 2.12(5), 1.90(3)] (Table 2).

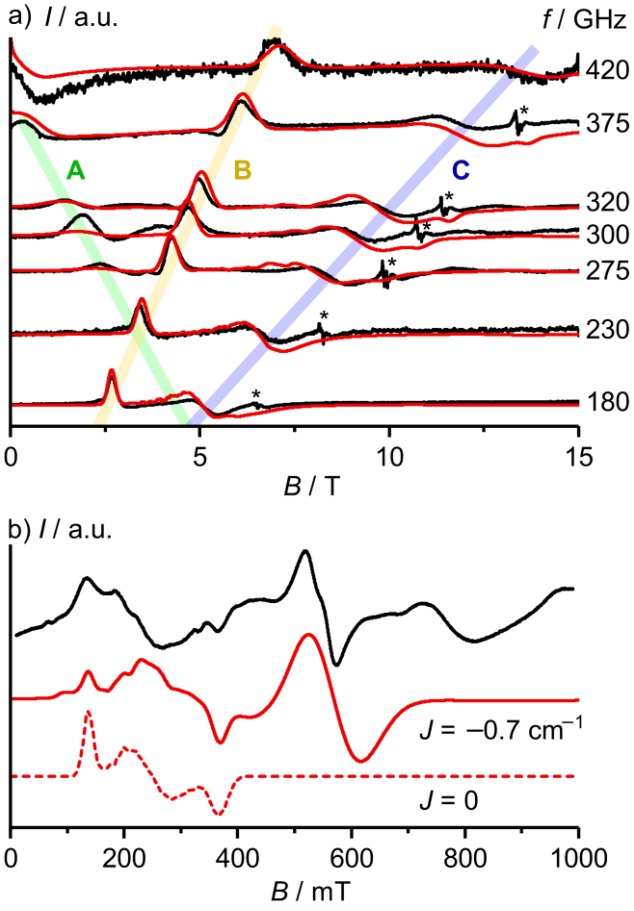

Figure 3: a) Frequency dependent HFEPR spectra (black trace) of *cisfac*-[**3**]$^{3+}$ (pressed pellet) at the indicated frequencies and 5 K with simulated spectra based on Eq. 1 (red trace). Colored lines (green, yellow, purple) added to guide the eye. Measurement artifacts arising from the instrumental setup are marked with asterisks. b) Powder X-band EPR spectrum of *cisfac*-[**3**]$^{3+}$ at 10 K (black trace) with simulated spectra based on Eq. 1 (red dashed trace) and Eq. S1 (red solid trace).

Since with HFEPR spectroscopy at constant temperature alone the sign of D cannot be determined with certainty, we recorded additional spectra at 320 GHz at variable temperatures (5–40 K, Figure S19). All three main signals A–C decrease in intensity with increasing temperature which suggests $D > 0$ and which is consistent with spin Hamiltonian simulations (see SI for details).

We completed the spectroscopic investigation of *cisfac*-[**3**]$^{3+}$ by solid state X-band EPR spectroscopy (9.6 GHz) at 10 K to cover transitions in the low energy region. We obtained a rich spectrum that can only be reasonably simulated by including an exchange interaction term[93] $JS_1{}^{T}S_2$ with a coupling constant of $J = -0.7$ cm^{-1} in Eq. 1 (Figure 3b). This hints to a small antiferromagnetic interaction between complex cations in the solid state or an impurity that forms over time when the air-sensitive complex decomposes. However, the simulated spectrum was not able to reproduce all signals that were found experimentally, indicating a more complex interaction scheme in *cisfac*-[**3**]$^{3+}$. We did not observe this coupling in the HFEPR spectra (Figure 3) because of the large line width of the signals and the high value of D compared to the magnitude of the interaction J (Table 2). Hence, the HFEPR spectra are dominated by signals arising from ZFS.

For a theoretical description of the ZFS in *cisfac*-**[3]$^{3+}$**, we performed complete active space self-consistent field calculations with spin-orbit coupling and *N*-electron valence state perturbation theory to correct for the missing dynamic electron correlation (SOC-CASSCF(7,12)-NEVPT2, see SI for details). The calculations yielded D = –6.6 cm^{-1} and E = 1.65 cm^{-1} which reasonably agrees with the magnitude of the experimental ZFS, but gives the wrong sign for D. The same behavior has been observed for the V^{II} analog of *cisfac*-**[3]$^{3+}$**, where the calculated ZFS parameters showed good agreement with experimental data for selected active spaces, while for others, the sign of D was inverted.[81]

In summary, SQUID magnetometry and EPR spectroscopy yield a consistent picture of the electronic ground state of *cisfac*-**[3]$^{3+}$** with a total electron spin S of $^3/_2$, ZFS parameters of D = 6.7(1) cm^{-1} and E = 0.8(5) cm^{-1}, $g_{xx,yy,zz}$ = [1.61(3), 2.12(5), 1.90(3)] and an exchange coupling constant of J = –0.7 cm^{-1} (Table 2). Literature reports on spin Hamiltonian parameters of monomeric molybdenum(III) complexes are scarce with many studies focusing on polynuclear compounds or clusters.[68,94,95] Apparent g-values were reported for Mo(acac)$_3$ (acac$^-$ = acetylacetonate), but the ZFS parameters were not explicitly considered in this analysis.[96] Another study only provided an estimate for the ZFS parameter $|D| > 1.5$ cm^{-1} for Mo(acac)$_3$.[97] A more detailed report found $g_{\parallel}$ = 1.94 and $g_{\perp}$ = 1.97 with D = –6.3 cm^{-1} and a small antiferromagnetic interaction (J = –0.65 cm^{-1}) for Mo(acac)$_3$ in the solid state which is similar to our results for *cisfac*-**[3]$^{3+}$**.[98] *Cisfac*-**[3]$^{3+}$** shows a higher ZFS than cyanide-bridged Mo–Ni complexes with $|D|$ values of 0.44 to 2.7 cm^{-1}.[99,100]

Optical Properties

The remarkable optical properties of *mer*-[Cr(ddpd)$_2$]$^{3+}$[14,25] inspired us to perform an in-depth optical characterization of *mer*-**1**, *mer*-**2** and *cisfac*-**[3]$^{3+}$**.

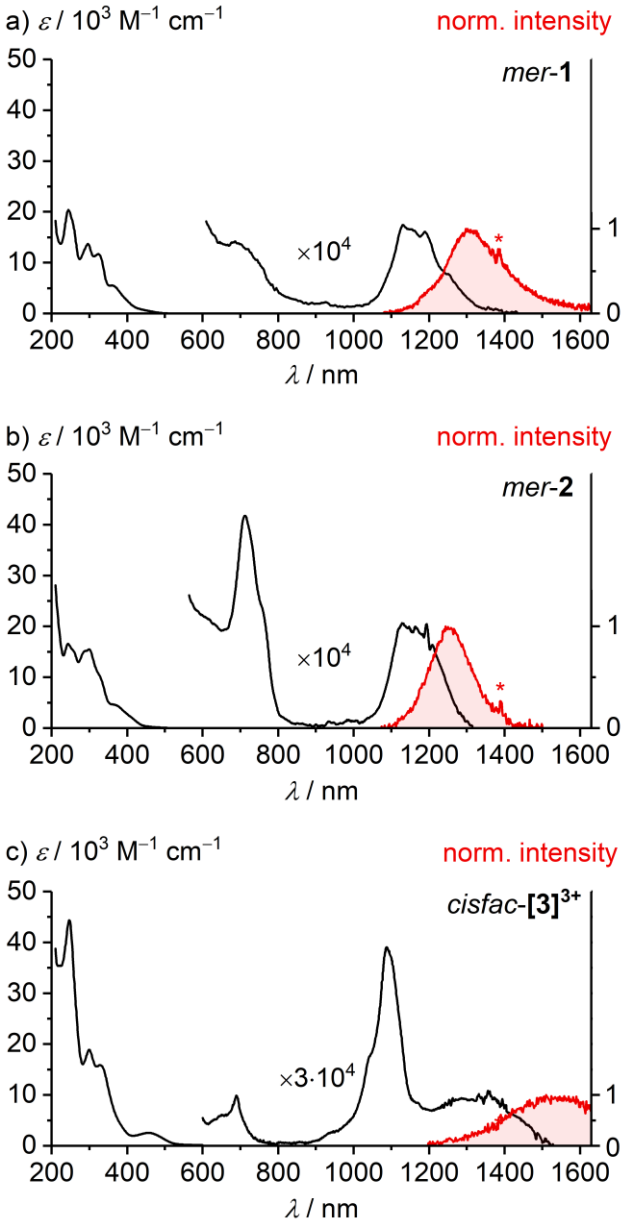

Figure 4: Absorption spectra (210–550 nm: MeCN, >550 nm: d_3-MeCN, black traces) and normalized photoluminescence spectra (λ_{exc} = 450 nm, MeCN, red traces, * = correction artifacts; see SI for details) of a) *mer*-**1**, b) *mer*-**2** and c) *cisfac*-**[3]**$^{3+}$. The weak low-energy absorption bands are scaled by a factor of a–b) 10^4 and c) $3{\cdot}10^4$.

All three complexes under investigation show intense absorptions in the UV to green spectral region that can be assigned to spin-allowed quartet transitions (Figure 4). The lowest energy transitions in this area have mainly quartet metal-to-ligand charge transfer ^{4}MLCT(Mo→ddpd) in *mer*-**1** and *mer*-**2**, and quartet ligand-to-metal charge transfer ^{4}LMCT(ddpd→Mo) character in *cisfac*-**[3]**$^{3+}$ according to TD-DFT calculations and charge transfer number analyses (Figure S20).[101] Higher-energy bands are of mixed quartet ligand-centered (^{4}LC), quartet ligand-to-ligand charge transfer (^{4}LL'CT) and ^{4}LMCT(X→Mo) character. As a sidenote, LC transitions only involve orbitals localized on a single ligand while LL'CT transitions involve a shift of electron density from one ligand to another. CASSCF(7,12)-NEVPT2 calculations place the lowest-energy $^4A_2$→$^4T_2$ transitions at 308, 423 and 452 nm for *cisfac*-**[3]**$^{3+}$, *mer*-**1** and *mer*-**2**, respectively. This reflects the decreasing ligand field splitting in this series in agreement with

the spectrochemical series $Br^- < Cl^- <$ pyridine (Figure S37–Figure S39). In the experimental absorption spectra, these formally Laporte-forbidden metal-centered transitions are masked by intense ^{4}LC and charge-transfer bands.

Table 3: Absorption band maxima λ_{abs} and molar absorption coefficients ε of *mer*-**1**, *mer*-**2** and *cisfac*-**[3]$^{3+}$**. Assignments drawn from TD-DFT calculations with charge transfer number analyses[101] and CASSCF(7,12)-NEVPT2 calculations (see SI for details). sh = shoulder.

mer-**1**		
λ_{abs} / nm	ε / M^{-1} cm^{-1}	assignment
245	20300	^{4}LC(ddpd)
296	13700	^{4}LC(ddpd), ^{4}(Cl→Mo)
324	11700	^{4}(Mo→ddpd), ^{4}LC(ddpd)
363	5500	^{4}(Mo→ddpd)
436	860	^{4}(Mo→ddpd)
693	1.4	$^4A_2$→$^2T_2$
748 (sh)	1.0	$^4A_2$→$^2T_2$
1130	1.7	$^4A_2$→$^2T_1$/^{2}E
1188	1.6	$^4A_2$→$^2T_1$/^{2}E
1268	0.6	$^4A_2$→$^2T_1$/^{2}E
mer-**2**		
λ_{abs} / nm	ε / M^{-1} cm^{-1}	assignment
244	16500	^{4}LC(ddpd)
257 (sh)	15300	^{4}LC(ddpd)
286 (sh)	15000	^{4}(Mo→ddpd), ^{4}LC(ddpd)
300	15500	^{4}(Br→Mo)
329 (sh)	10000	^{4}LC(ddpd)
369	4500	^{4}(Mo→ddpd)
413 (sh)	2000	^{4}LC(ddpd)
712	4.2	$^4A_2$→$^2T_2$
760 (sh)	2.3	$^4A_2$→$^2T_2$
1130	2.1	$^4A_2$→$^2T_1$/^{2}E
1188	1.8	$^4A_2$→$^2T_1$/^{2}E
cisfac-**[3]$^{3+}$**		
λ_{abs} / nm	ε / M^{-1} cm^{-1}	assignment
246	44400	^{4}LC(ddpd)
299	18800	^{4}LC(ddpd)
328	15900	^{4}LC(ddpd), ^{4}LL'CT
457	2540	^{4}LMCT
650	0.2	$^4A_2$→$^2T_2$
691	0.3	$^4A_2$→$^2T_2$
936	0.08	$^4A_2$→$^2T_1$/^{2}E
1040	0.6	$^4A_2$→$^2T_1$/^{2}E
1087	1.3	$^4A_2$→$^2T_1$/^{2}E
1325	0.3	$^4A_2$→$^2T_1$

Concentrated solutions of *mer*-**1**, *mer*-**2** and *cisfac*-**[3]$^{3+}$** in d_3-MeCN revealed two sets of weak absorption bands in the red and near-infrared (NIR) spectral region that we assign to the spin-flip transitions $^4A_2$→$^2T_2$ and $^4A_2$→$^2T_1$/^{2}E, respectively, using CASSCF(7,12)-NEVPT2

calculations (Figure 4, Table 3, see SI for details). The strong spin-orbit coupling induced by heavy atoms such as Mo and Br lifts the spin selection rule rendering these formally spin- and Laporte-forbidden transitions relatively strong (ε = 0.3–4.2 M^{-1} cm^{-1}) and most intense in *mer*-**2**. The weakest spin-forbidden absorptions were found for *cisfac*-**[3]$^{3+}$** because the Laporte rule applies more strongly in this case due to the higher local symmetry of the [MoN_6] core. In contrast to the heteroleptic complexes, *cisfac*-**[3]$^{3+}$** features a broad absorption band at 1200–1500 nm that we assign to a more strongly distorted state of $^2T_1$ parentage. Overall, the energies of the spin-forbidden transitions are hardly affected by the ligand environment. While CASSCF(7,12)-NEVPT2 calculations overestimate the absolute transition energies by *ca.* 2000–3000 cm^{-1}, they correctly reflect the higher spread of $^2T_1/^2E$ states in *cisfac*-**[3]$^{3+}$** compared to *mer*-**1** and *mer*-**2** (Figure S50). For *mer*-**1** and *mer*-**2**, the multi-reference calculations on the Franck-Condon geometry place a ^2E state at lowest energy, while for *cisfac*-**[3]$^{3+}$** the lowest doublet state is $^2T_1$ in character. The calculations also predict a minor influence of the specific configuration of the ddpd ligands in **[3]$^{3+}$** (*cisfac*, *transfac* or *mer*) on the energies of the doublet states (Figure S50). There is, however, a notable shift of the two states of ^2E parentage to higher energy in the two facial isomers (Figure S50).

In previous reports *e.g.* on the ddpd complexes of chromium(III)[40] and vanadium(II),[81] the position of the metal-centered $^4A_2 \rightarrow {}^4T_2$ absorption bands that correspond to the ligand field splitting was identified using magnetic circular dichroism (MCD) supplemented by CASSCF calculations. So in an attempt to better resolve the energetically close-lying electronic transitions in *cisfac*-**[3]$^{3+}$**, we measured recorded its MCD response at 1.8 K and 5 T (Figure S22). The spectrum was deconvoluted with Gaussian curves yielding seven components (Figure S22, Table S12) revealing a fine-structure of the ^{4}LMCT band at 450 nm. However, the simulated MCD spectrum obtained from CASSCF(7,7)-NEVPT2 calculations did not match the experiment (Figure S23). This is likely because the metal-centered $^4A_2 \rightarrow {}^4T_2$ transitions are hidden under MCD bands originating from ^{4}CT states, which limits further analysis of the data in this regard.

Excitation of *mer*-**1**, *mer*-**2** and *cisfac*-**[3]$^{3+}$** with a blue cw-laser (450 nm) in MeCN solution at room temperature reveals weak emission bands peaking at 1300, 1250 and 1550 nm, with full widths at half maximum (FWHM) of 980, 840 and *ca.* 1200 cm^{-1}, respectively (Figure 4, Table 4, Figure S24). The Stokes shifts of 600–1000 cm^{-1} indicate a small but significant excited state distortion in all three complexes that is also reflected in the respective DFT-optimized geometries of optimized metal-centered doublet states (Figure S51, Table S14). Hence, we assign the emission to spin-flip phosphorescence from slightly distorted $^2T_1$ states. *Mer*-[$Cr(ddpd)_2$]$^{3+}$ only showed small Stokes shifts (<100 cm^{-1}) and sharper bands (FWHM = 420 cm^{-1}) in comparison,[14] which might reflect the higher flexibility of the first coordination sphere around the larger molybdenum(III) ion in *mer*-**1**, *mer*-**2** and *cisfac*-**[3]$^{3+}$**. In contrast to most Cr^{III} complexes,[24,35] emission of *mer*-**1**, *mer*-**2** and *cisfac*-**[3]$^{3+}$** was only detected from their lowest-energy doublet states, although the $^2T_1/^2E$ states are most likely thermally equilibrated due to being close in energy. We speculate that the spin-flip transitions from higher-lying doublet states have lower radiative rates, and are therefore difficult to detect.

In the solid state, *mer*-**1**, *mer*-**2** and *cisfac*-**[3]**[BF_4]$_3$ show significantly more intense luminescence with 450 nm excitation (cw-laser, 1 W) that is only slightly shifted with regards to the data obtained in solution (Figure S29, Figure S30, Figure S31, Table 4). The luminescence intensity of *cisfac*-**[3]**[BF_4]$_3$ increased by *ca.* one order of magnitude upon

cooling of the sample to 77 K (Figure S32) suggesting a thermally activated relaxation pathway. Additional emission bands peaking at 900–1130 nm were assigned to artifacts that arise from reabsorption of a luminescence background by the spin-forbidden transitions (Figure S33, Figure S34, see general methods section in SI). The luminescence lifetimes of *mer*-**1** and *mer*-**2** in the solid state were determined as 24±10 and 15±5 ns, respectively. Further luminescence lifetimes or quantum yield measurements are precluded by the generally weak luminescence intensity. From our experience with other samples measured in our spectrometer, we estimate the quantum yields of *mer*-**1**, *mer*-**2** and *cisfac*-**[3]**$^{3+}$ in MeCN and the solid state at room temperature to be below 0.00001 %.

Table 4: Spin-flip phosphorescence band maxima λ_{max} of *mer*-**1**, *mer*-**2** and *cisfac*-**[3]**$^{3+}$ in MeCN at room temperature and in the solid state with luminescence lifetime τ in the solid state.

Complex	λ_{max} (MeCN) / nm	λ_{max} (solid) / nm	τ (solid) / ns	assignment
mer-**1**	1310	1300	24±10	$^2T_1 \rightarrow {}^4A_2$
mer-**2**	1250	1270	15±5	$^2T_1 \rightarrow {}^4A_2$
cisfac-**[3]**$^{3+}$	1550	1510	–	$^2T_1 \rightarrow {}^4A_2$

The photostability of the complexes in MeCN under cw-laser irradiation at 450 nm (1 W) qualitatively decreases in the order *cisfac*-**[3]**$^{3+}$ ≫ *mer*-**1** > *mer*-**2**. The emission spectra of *mer*-**1** do not change in consecutive scans, but the complex decomposes after 14 min of irradiation (Figure S27a). Irradiation of *mer*-**2** readily decomposes to a species emitting at 1530 nm (Figure S25, Figure S27b). Mass spectrometric analysis of a photolyzed sample of *mer*-**2** suggests loss of bromide forming $MoBr_2$(ddpd)(MeCN) (Figure S26). *Cisfac*-**[3]**$^{3+}$ is very photostable and does not decompose after 40 min of irradiation (Figure S27c). None of the three complexes showed signs of photodegradation in the solid state under air.

Mer-**1** and *mer*-**2** emit at lower energies than *fac*-$MoX_3(Me_3[9]aneN_3)$ (X = Cl, Br, $Me_3[9]aneN_3$ = 1,4,7-trimethyl-1,4,7-triazacyclononane) with phosphorescence band maxima at 1120 and 1130 nm, respectively.[70] This can be explained by a stronger nephelauxetic effect induced by the 'softer' aromatic ddpd ligand compared to the 'harder' amine-based ligand $Me_3[9]aneN_3$. A similar blue-shift of the emission can be observed for comparable Cr^{III} complexes with pyridine and amine ligands.[24] *Cisfac*-**[3]**$^{3+}$ is the first example for a luminescent molybdenum(III) complex solely stabilized by polypyridyl ligands, and shows the lowest spin-flip emission energy reported so far.[24] This suggests an unexpectedly high covalency between the metal and the ddpd ligands.[24] Emission in this low energy region is very rarely observed from transition metal complexes[102,103] and more commonly found for *ff*-transitions of lanthanides.[104,105]

Deactivation of low-energy luminescence can occur via energy transfer to vibrational overtones of the ligand or solvent with a distance dependence of r^{-6}.[33,34] Given that the emission bands of *mer*-**1**, *mer*-**2** and *cisfac*-**[3]**$^{3+}$ overlap with NIR absorption bands of acetonitrile at 1170 and 1380 nm originating from vibrational overtones (Figure S28),[106] it is surprising that the luminescence is detectable at all, even in solution at room temperature. Possibly, the metal-confined nature of the spin-flip states hinders quenching *via* this intermolecular pathway. Apart from the solvent, the coordinated ddpd ligand presents C–H oscillators in close proximity to the

metal center. The emission bands of *mer*-**1** and *mer*-**2** are located between the first (v^2) and second (v^3) C–H vibrational overtones of the ligand (1670 and 1136 nm),[34] while the emission band of *cisfac*-**[3]**$^{3+}$ significantly overlaps with the first overtone v^2(C–H) (Figure S28). Hence, we expect ligand deuteration to strongly enhance phosphorescence lifetimes and quantum yields in *mer*-**1**, *mer*-**2** and especially *cisfac*-**[3]**$^{3+}$, in analogy to reports on chromium(III) complexes.[29,34] Work along these lines is currently in progress in our labs.

Excited state dynamics of *cisfac*-[3]$^{3+}$

To elucidate the temporal evolution of the excited states in *cisfac*-**[3]**$^{3+}$ we recorded fs-transient absorption (TA) spectra after pulsed ^{4}LMCT excitation at 515 nm in MeCN (Figure 5, Figure S53). The TA spectra bear some similarity with those obtained for [Cr(ddpd)$_2$]$^{3+}$.[14] Global analysis of the data reveals three time constants for *cisfac*-**[3]**$^{3+}$ (τ_1 = 2.5 ps, τ_2 = 6.2 ps, τ_3 = 1.4 ns, Figure S53, Figure S55, Figure S56). The initial spectrum shows an intense excited state absorption at 740 nm that decays to a new species within 2.5 ps with absorption maxima at 525 and 660 nm. The pseudo-isosbestic point in the area-normalized TA spectra suggests that this transition proceeds from one state to the other, or *via* intermediate states that do not accumulate (Figure S57).[107] Hence, we assign this process to the transition from the initially excited ^{4}LMCT state to the spin-flip states (^{2}T$_2$/^{2}T$_1$/^{2}E) with an upper limit for the time constant for intersystem crossing (ISC) τ_{ISC} of 2.5 ps. This is in line with a recent study on a chromium(III) complex where it was not possible to isolate the ISC process with TA spectroscopy alone.[108]

Next, the bands sharpen and shift to higher energy with a time constant of 6.2 ps which is consistent with internal conversion (IC) and vibrational cooling (VC) within the doublet excited states ^{2}T$_1$/^{2}E (Figure S58). After 17 ps, the shape of the TA spectra does not change significantly anymore (Figure S58) and the ^{2}T$_1$/^{2}E states decay to the ^{4}A$_2$ ground state with a time constant of τ = 1.4 ns.

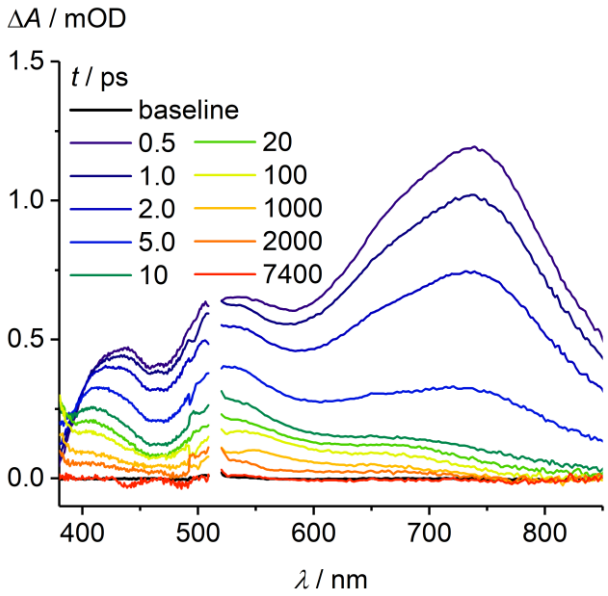

Figure 5: Transient absorption spectra of *cisfac*-**[3]**$^{3+}$ in MeCN after pulsed excitation at 515 nm at various time delays (fluence: 35 µJ cm^{-2}, repetition rate: 50 kHz). Spectral window of 509–520 nm was omitted for clarity due to excitation scatter.

The decay of the $^2E/^2T_1$ states in *cisfac*-**[3]**$^{3+}$ (τ = 1.4 ns) is six orders of magnitude faster than in *mer*-$[Cr(ddpd)_2]^{3+}$ (τ = 1.12 ms) for which we propose four main reasons: 1) The energy of the $^2T_1/^2E$ states in *cisfac*-**[3]**$^{3+}$ is *ca.* 0.7 eV lower than that of the chromium(III) complex which facilitates non-radiative relaxation according to the energy gap law.[48] 2) Multi-phonon relaxation *via* vibrational overtones of the ligand is favored for *cisfac*-**[3]**$^{3+}$ as its emission overlaps with the ν^2(C–H) band of the pyridyl ligand (Figure S28), while the much weaker ν^4 and ν^5 overtones are relevant for *mer*-$[Cr(ddpd)_2]^{3+}$.[33,34] 3) The high spin-orbit coupling in *cisfac*-**[3]**$^{3+}$ induced by the 4d ion Mo^{III}[74] accelerates formally spin-forbidden processes such as the $^2T_1/^2E \rightarrow {}^4A_2$ relaxation.[109–112] 4) The cis-facial coordination of ddpd in *cisfac*-**[3]**$^{3+}$ enables trigonal distortions in the excited doublet states which can lead to non-radiative deactivation *via* low-energy mixed states, and which are not available in the more rigid *mer*-$[Cr(ddpd)_2]^{3+}$.[24,113] It is worth noting that the $^4T_2$ states that are central to the design of chromium(III) complexes are irrelevant for the photophysics in molybdenum(III) complexes because of their intrinsically much higher energy (Figure 6).

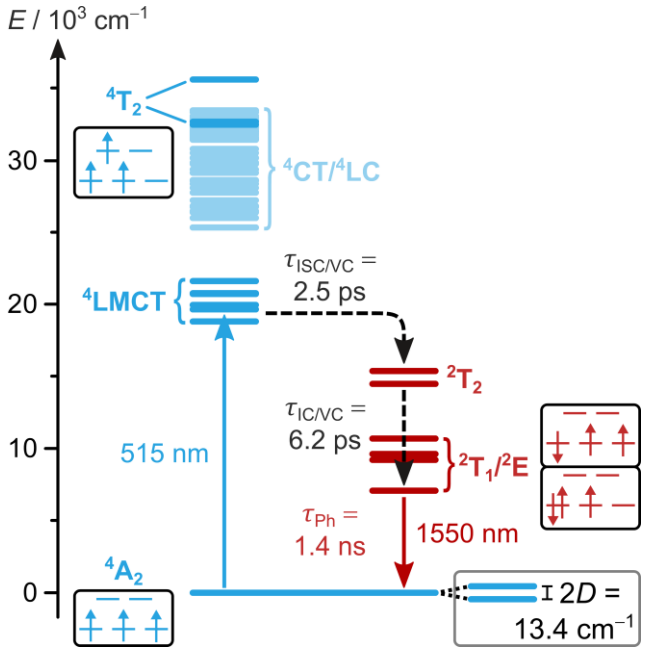

Figure 6: Energy diagram of *cisfac*-**[3]**$^{3+}$ with microstates of electronically excited states, with time constants τ for the excited state dynamics determined by TA spectroscopy (MeCN, λ_{exc} = 515 nm) and ZFS (2*D*) determined by HFEPR spectroscopy (not to scale, gray box). The blue bars on the left indicate the quartet ground state and the lowest quartet excited states as obtained from TD-DFT (^{4}CT/^{4}LC) and CASSCF(7,12)-NEVPT2 calculations ($^4T_2$). The metal-centered $^4T_2$ states are buried under ^{4}CT and ^{4}LC transitions. The red bars correspond to the doublet spin-flip states whose energies were extracted from absorption and emission spectra.

Conclusions

While phosphorescence from metal-centered spin-flip states in chromium(III) complexes is well understood[15,22,25,29,30,38,45,46,114,115] the effects of combining the ligand ddpd with the heavier molybdenum(III) as central ion had not been delineated yet. The new water and oxygen-sensitive complexes *mer*-MoX_3(ddpd) (X = Cl, Br) and *cisfac*-$[Mo(ddpd)_2]^{3+}$ showed weak low-energy phosphorescence in the NIR-II in solution at room temperature. The excited state lifetime of *cisfac*-$[Mo(ddpd)_2]^{3+}$ (1.4 ns) was found to be six orders of magnitude shorter than that of *mer*-$[Cr(ddpd)_2]^{3+}$ (1.12 ms).[26] SQUID magnetometry and EPR spectroscopy on *cisfac*-

$[Mo(ddpd)_2]^{3+}$ revealed large zero-field splitting parameters of D = 6.7(1) cm^{-1} and E = 0.8(5) cm^{-1} compared to chromium(III)[40] resulting from strong spin-orbit coupling.

As suspected, it is not possible to simply transfer the learnings from chromium(III) photophysics[14,111] to its heavy cousin molybdenum(III). Instead our results suggest the following guidelines for the future design of photoactive molybdenum(III) complexes: 1) Unlike with chromium(III),[14] dedicated strong-field ligands are not required to avoid deactivation *via* back-intersystem crossing. Even in the heteroleptic complexes MoX_3(ddpd) with the weak, π-donating chlorido and bromido ligands, the ligand field splitting was sufficiently large. 2) Ligands should be selected for a weak nephelauxetic effect, forming more ionic Mo–L bonds, to push the emissive spin-flip states to higher energies. 3) High-energy oscillators (C–H, N–H, O–H) in close proximity to the metal center should be avoided to reduce multi-phonon relaxation, either by ligand design or by ligand deuteration. 4) Rigid ligands, preferably in meridional configuration can help to limit deactivation of the excited states *via* trigonal distortion. 5) Shielding of the metal center from nucleophilic attacks can increase the overall stability against oxidation and hydrolysis.

We are confident that these guardrails can keep us on the road to stable molybdenum(III) complexes with sharp NIR-II luminescence beyond materials based on rare-earth metals.

Supporting Information

The Supporting Information is available free of charge at xx.

Supporting Information: General methods, synthetic procedures, mass spectra, crystal structure parameters, cyclic voltammetry, spectroscopic data (FTIR, XAS, EPR, UV/Vis absorption, MCD, luminescence, fs-transient absorption), quantum chemical calculations (PDF). Cartesian coordinates of geometries optimized using quantum chemical calculations (XYZ).

Acknowledgements

The authors thank Dr. Dieter Schollmeyer for the collection of X-ray diffraction data, Dr. Christopher Kampf for the acquisition of the mass spectra, Dr. Jens Kalmbach and Prof. Dr. Michael Seitz (Tübingen University) for preliminary luminescence measurements and Dr. Robert Naumann for support during TA data analysis. WRK is grateful for financial support by the German Academic Scholarship Foundation (Studienstiftung des Deutschen Volkes), by the Chemical Industry Funds (Fonds der Chemischen Industrie, FCI) and by the Max Planck Graduate Center with the Johannes Gutenberg University Mainz (MPGC). APMR and SF are grateful for financial support from Harvard University's Rowland Institute. The authors thank the German Research Foundation (DFG) through grant INST 247/1018-1 FUGG to KH and the Priority Program SPP 2102 "Light-controlled reactivity of metal complexes" HE2778/15-1 and BA 4467/7-1. Provision of beamtime by PETRA III (DESY) at beamline P65 and support by the beamline staff is acknowledged. Parts of this research were conducted using the supercomputers Mogon and Elwetritsch and advisory services offered by Johannes Gutenberg University, Mainz (https://hpc.uni-mainz.de), and the University of Kaiserslautern-Landau (https://hpc.rz.rptu.de), which are members of the AHRP and the Gauss Alliance e.V.

Author contributions

WRK synthesized the complexes, performed the optical characterization, the quantum chemical calculations, analyzed the TA data, and wrote the manuscript. DH performed HFEPR, X-band

EPR, SQUID and MCD measurements, analyzed the data and wrote parts of the manuscript, supervised by JvS. CF solved and refined the crystal structures. RS recorded EXAFS spectra and analyzed the data, supervised by MB. APMR recorded and analyzed TA data, supervised by SF. KH conceptualized and supervised the entire study. The manuscript was written through contributions of all authors. All authors have given approval to the final version of the manuscript.

References

(1) DiLuzio, S.; Mdluli, V.; Connell, T. U.; Lewis, J.; VanBenschoten, V.; Bernhard, S. High-Throughput Screening and Automated Data-Driven Analysis of the Triplet Photophysical Properties of Structurally Diverse, Heteroleptic Iridium(III) Complexes. *J. Am. Chem. Soc.* **2021**, *143* (2), 1179–1194. DOI: 10.1021/jacs.0c12290.

(2) Burstall, F. H. Optical activity dependent on co-ordinated bivalent ruthenium. *J. Chem. Soc.* **1936**, 173–175. DOI: 10.1039/JR9360000173.

(3) King, K. A.; Spellane, P. J.; Watts, R. J. Excited-state properties of a triply ortho-metalated iridium(III) complex. *J. Am. Chem. Soc.* **1985**, *107* (5), 1431–1432. DOI: 10.1021/ja00291a064.

(4) Thompson, D. W.; Ito, A.; Meyer, T. J. $[Ru(bpy)_3]^{2+}$* and other remarkable metal-to-ligand charge transfer (MLCT) excited states. *Pure Appl. Chem.* **2013**, *85* (7), 1257–1305. DOI: 10.1351/PAC-CON-13-03-04.

(5) Juris, A.; Balzani, V.; Barigelletti, F.; Campagna, S.; Belser, P.; Zelewsky, A. von. Ru(II) polypyridine complexes: photophysics, photochemistry, eletrochemistry, and chemiluminescence. *Coord. Chem. Rev.* **1988**, *84*, 85–277. DOI: 10.1016/0010-8545(88)80032-8.

(6) Li, X.; Xie, Y.; Li, Z. Diversity of Luminescent Metal Complexes in OLEDs: Beyond Traditional Precious Metals. *Chem. Asian J.* **2021**, *16* (19), 2817–2829. DOI: 10.1002/asia.202100784.

(7) Wenger, O. S. Is Iron the New Ruthenium? *Chem. Eur. J.* **2019**, *25* (24), 6043–6052. DOI: 10.1002/chem.201806148.

(8) Förster, C.; Heinze, K. Photophysics and photochemistry with Earth-abundant metals - fundamentals and concepts. *Chem. Soc. Rev.* **2020**, *49*, 1057–1070. DOI: 10.1039/C9CS00573K.

(9) Wenger, O. S. Photoactive Complexes with Earth-Abundant Metals. *J. Am. Chem. Soc.* **2018**, *140* (42), 13522–13533. DOI: 10.1021/jacs.8b08822.

(10) Wegeberg, C.; Wenger, O. S. Luminescent First-Row Transition Metal Complexes. *JACS Au* **2021**, *1* (11), 1860–1876. DOI: 10.1021/jacsau.1c00353.

(11) Sinha, N.; Wenger, O. S. Photoactive Metal-to-Ligand Charge Transfer Excited States in $3d^6$ Complexes with Cr^0, Mn^I, Fe^{II}, and Co^{III}. *J. Am. Chem. Soc.* **2023**, *145* (9), 4903–4920. DOI: 10.1021/jacs.2c13432.

(12) Herr, P.; Kerzig, C.; Larsen, C. B.; Häussinger, D.; Wenger, O. S. Manganese(I) complexes with metal-to-ligand charge transfer luminescence and photoreactivity. *Nat. Chem.* **2021**, *13* (10), 956–962. DOI: 10.1038/s41557-021-00744-9.

(13) Herr, P.; Glaser, F.; Büldt, L. A.; Larsen, C. B.; Wenger, O. S. Long-Lived, Strongly Emissive, and Highly Reducing Excited States in Mo(0) Complexes with Chelating Isocyanides. *J. Am. Chem. Soc.* **2019**, *141* (36), 14394–14402. DOI: 10.1021/jacs.9b07373.

(14) Kitzmann, W. R.; Ramanan, C.; Naumann, R.; Heinze, K. Molecular ruby: exploring the excited state landscape. *Dalton. Trans.* **2022**, *51* (17), 6519–6525. DOI: 10.1039/d2dt00569g.

(15) Bürgin, T. H.; Glaser, F.; Wenger, O. S. Shedding Light on the Oxidizing Properties of Spin-Flip Excited States in a Cr^{III} Polypyridine Complex and Their Use in Photoredox Catalysis. *J. Am. Chem. Soc.* **2022**, *144* (31), 14181–14194. DOI: 10.1021/jacs.2c04465.
(16) Welin, E. R.; Le, C.; Arias-Rotondo, D. M.; McCusker, J. K.; MacMillan, D. W. C. Photosensitized, energy transfer-mediated organometallic catalysis through electronically excited nickel(II). *Science* **2017**, *355* (6323), 380–385. DOI: 10.1126/science.aal2490.
(17) Kaufhold, S.; Rosemann, N. W.; Chábera, P.; Lindh, L.; Bolaño Losada, I.; Uhlig, J.; Pascher, T.; Strand, D.; Wärnmark, K.; Yartsev, A.; Persson, P. Microsecond Photoluminescence and Photoreactivity of a Metal-Centered Excited State in a Hexacarbene-Co(III) Complex. *J. Am. Chem. Soc.* **2021**, *143* (3), 1307–1312. DOI: 10.1021/jacs.0c12151.
(18) Kjær, K. S.; Kaul, N.; Prakash, O.; Chábera, P.; Rosemann, N. W.; Honarfar, A.; Gordivska, O.; Fredin, L. A.; Bergquist, K.-E.; Häggström, L.; Ericsson, T.; Lindh, L.; Yartsev, A.; Styring, S.; Huang, P.; Uhlig, J.; Bendix, J.; Strand, D.; Sundström, V.; Persson, P.; Lomoth, R.; Wärnmark, K. Luminescence and reactivity of a charge-transfer excited iron complex with nanosecond lifetime. *Science* **2019**, *363* (6424), 249–253. DOI: 10.1126/science.aau7160.
(19) East, N.; Naumann, R.; Förster, C.; Ramanan, C.; Diezemann, G.; Heinze, K. Oxidative Two-State Photoreactivity of a Manganese(IV) Complex using NIR Light. *chemRxiv (Preprint)* **2023.** DOI: 10.26434/chemrxiv-2023-bhl82.
(20) Sharma, N.; Jung, J.; Ohkubo, K.; Lee, Y.-M.; El-Khouly, M. E.; Nam, W.; Fukuzumi, S. Long-Lived Photoexcited State of a Mn(IV)-Oxo Complex Binding Scandium Ions That is Capable of Hydroxylating Benzene. *J. Am. Chem. Soc.* **2018**, *140* (27), 8405–8409. DOI: 10.1021/jacs.8b04904.
(21) Förster, C.; Heinze, K. Bimolecular reactivity of 3d metal-centered excited states (Cr, Mn, Fe, Co). *Chem. Phys. Rev.* **2022**, *3* (4), 41302. DOI: 10.1063/5.0112531.
(22) Wang, C.; Reichenauer, F.; Kitzmann, W. R.; Kerzig, C.; Heinze, K.; Resch-Genger, U. Efficient Triplet-Triplet Annihilation Upconversion Sensitized by a Chromium(III) Complex via an Underexplored Energy Transfer Mechanism. *Angew. Chem. Int. Ed.* **2022**, *61* (27), e202202238. DOI: 10.1002/anie.202202238.
(23) Scattergood, P. A. Recent advances in chromium coordination chemistry: luminescent materials and photocatalysis. In *Organometallic Chemistry*; Patmore, N. J., Elliott, P. I. P., Eds.; Organometallic Chemistry; Royal Society of Chemistry, 2020; pp 1–34. DOI: 10.1039/9781788017077-00001.
(24) Kitzmann, W. R.; Moll, J.; Heinze, K. Spin-flip luminescence. *Photochem. Photobiol. Sci.* **2022**, *21* (7), 1309–1331. DOI: 10.1007/s43630-022-00186-3.
(25) Otto, S.; Grabolle, M.; Förster, C.; Kreitner, C.; Resch-Genger, U.; Heinze, K. $[Cr(ddpd)_2]^{3+}$ A Molecular, Water-Soluble, Highly NIR-Emissive Ruby Analogue. *Angew. Chem. Int. Ed.* **2015**, *54* (39), 11572–11576. DOI: 10.1002/anie.201504894.
(26) Wang, C.; Kitzmann, W. R.; Weigert, F.; Förster, C.; Wang, X.; Heinze, K.; Resch-Genger, U. Matrix Effects on Photoluminescence and Oxygen Sensitivity of a Molecular Ruby. *ChemPhotoChem* **2022**, *6* (6), e202100296. DOI: 10.1002/cptc.202100296.
(27) Förster, C.; Dorn, M.; Reuter, T.; Otto, S.; Davarci, G.; Reich, T.; Carrella, L.; Rentschler, E.; Heinze, K. Ddpd as Expanded Terpyridine:Dramatic Effects of Symmetry and Electronic Properties in First Row Transition Metal Complexes. *Inorganics* **2018**, *6* (3), 86. DOI: 10.3390/inorganics6030086.

(28) Sinha, N.; Yaltseva, P.; Wenger, O. S. The Nephelauxetic Effect Becomes an Important Design Factor for Photoactive First-Row Transition Metal Complexes. *Angew. Chem. Int. Ed.* **2023**, *62* (30), e202303864. DOI: 10.1002/anie.202303864.
(29) Reichenauer, F.; Wang, C.; Förster, C.; Boden, P.; Ugur, N.; Báez-Cruz, R.; Kalmbach, J.; Carrella, L. M.; Rentschler, E.; Ramanan, C.; Niedner-Schatteburg, G.; Gerhards, M.; Seitz, M.; Resch-Genger, U.; Heinze, K. Strongly Red-Emissive Molecular Ruby $[Cr(bpmp)_2]^{3+}$ Surpasses $[Ru(bpy)_3]^{2+}$. *J. Am. Chem. Soc.* **2021**, *143* (30), 11843–11855. DOI: 10.1021/jacs.1c05971.
(30) Sinha, N.; Jiménez, J.-R.; Pfund, B.; Prescimone, A.; Piguet, C.; Wenger, O. S. A Near-Infrared-II Emissive Chromium(III) Complex. *Angew. Chem. Int. Ed.* **2021**, *60* (44), 23722–23728. DOI: 10.1002/anie.202106398.
(31) Stein, L.; Boden, P.; Naumann, R.; Förster, C.; Niedner-Schatteburg, G.; Heinze, K. The overlooked NIR luminescence of $Cr(ppy)_3$. *Chem. Commun.* **2022**, *58* (22), 3701–3704. DOI: 10.1039/D2CC00680D.
(32) Sawicka, N.; Craze, C. J.; Horton, P. N.; Coles, S. J.; Richards, E.; Pope, S. J. A. Long-lived, near-IR emission from Cr(III) under ambient conditions. *Chem. Commun.* **2022**, *58* (38), 5733–5736. DOI: 10.1039/D2CC01434C.
(33) Browne, W. The effect of deuteriation on the emission lifetime of inorganic compounds. *Coord. Chem. Rev.* **2001**, *219-221*, 761–787. DOI: 10.1016/S0010-8545(01)00366-6.
(34) Wang, C.; Otto, S.; Dorn, M.; Kreidt, E.; Lebon, J.; Sršan, L.; Di Martino-Fumo, P.; Gerhards, M.; Resch-Genger, U.; Seitz, M.; Heinze, K. Deuterated Molecular Ruby with Record Luminescence Quantum Yield. *Angew. Chem. Int. Ed.* **2018**, *57* (4), 1112–1116. DOI: 10.1002/anie.201711350.
(35) Otto, S.; Scholz, N.; Behnke, T.; Resch-Genger, U.; Heinze, K. Thermo-Chromium: A Contactless Optical Molecular Thermometer. *Chem. Eur. J.* **2017**, *23* (50), 12131–12135. DOI: 10.1002/chem.201701726.
(36) Otto, S.; Harris, J. P.; Heinze, K.; Reber, C. Molecular Ruby under Pressure. *Angew. Chem. Int. Ed.* **2018**, *57* (34), 11069–11073. DOI: 10.1002/anie.201806755.
(37) Otto, S.; Nauth, A. M.; Ermilov, E.; Scholz, N.; Friedrich, A.; Resch-Genger, U.; Lochbrunner, S.; Opatz, T.; Heinze, K. Photo-Chromium: Sensitizer for Visible-Light-Induced Oxidative C−H Bond Functionalization-Electron or Energy Transfer? *ChemPhotoChem* **2017**, *1* (8), 344–349. DOI: 10.1002/cptc.201700077.
(38) Sittel, S.; Naumann, R.; Heinze, K. Molecular Rubies in Photoredox Catalysis. *Front. Chem.* **2022**, *10*, 887439. DOI: 10.3389/fchem.2022.887439.
(39) Kalmbach, J.; Wang, C.; You, Y.; Förster, C.; Schubert, H.; Heinze, K.; Resch-Genger, U.; Seitz, M. Near-IR to Near-IR Upconversion Luminescence in Molecular Chromium Ytterbium Salts. *Angew. Chem. Int. Ed.* **2020**, *59* (42), 18804–18808. DOI: 10.1002/anie.202007200.
(40) Lenz, S.; Bamberger, H.; Hallmen, P. P.; Thiebes, Y.; Otto, S.; Heinze, K.; van Slageren, J. Chromium(III)-based potential molecular quantum bits with long coherence times. *Phys. Chem. Chem. Phys.* **2019**, *21* (13), 6976–6983. DOI: 10.1039/C9CP00745H.
(41) Fataftah, M. S.; Zadrozny, J. M.; Coste, S. C.; Graham, M. J.; Rogers, D. M.; Freedman, D. E. Employing Forbidden Transitions as Qubits in a Nuclear Spin-Free Chromium Complex. *J. Am. Chem. Soc.* **2016**, *138* (4), 1344–1348. DOI: 10.1021/jacs.5b11802.
(42) Bayliss, S. L.; Laorenza, D. W.; Mintun, P. J.; Kovos, B. D.; Freedman, D. E.; Awschalom, D. D. Optically addressable molecular spins for quantum information processing. *Science* **2020**, *370* (6522), 1309–1312. DOI: 10.1126/science.abb9352.

(43) Fataftah, M. S.; Bayliss, S. L.; Laorenza, D. W.; Wang, X.; Phelan, B. T.; Wilson, C. B.; Mintun, P. J.; Kovos, B. D.; Wasielewski, M. R.; Han, S.; Sherwin, M. S.; Awschalom, D. D.; Freedman, D. E. Trigonal Bipyramidal V^{3+} Complex as an Optically Addressable Molecular Qubit Candidate. *J. Am. Chem. Soc.* **2020**, *142* (48), 20400–20408. DOI: 10.1021/jacs.0c08986.
(44) Dee, C.; Zinna, F.; Kitzmann, W. R.; Pescitelli, G.; Heinze, K.; Di Bari, L.; Seitz, M. Strong circularly polarized luminescence of an octahedral chromium(III) complex. *Chem. Commun.* **2019**, *55* (87), 13078–13081. DOI: 10.1039/C9CC06909G.
(45) Jiménez, J.-R.; Doistau, B.; Cruz, C. M.; Besnard, C.; Cuerva, J. M.; Campaña, A. G.; Piguet, C. Chiral Molecular Ruby $[Cr(dqp)_2]^{3+}$ with Long-Lived Circularly Polarized Luminescence. *J. Am. Chem. Soc.* **2019**, *141*, 13244–13252. DOI: 10.1021/jacs.9b06524.
(46) Jiménez, J.-R.; Poncet, M.; Míguez-Lago, S.; Grass, S.; Lacour, J.; Besnard, C.; Cuerva, J. M.; Campaña, A. G.; Piguet, C. Bright Long-Lived Circularly Polarized Luminescence in Chiral Chromium(III) Complexes. *Angew. Chem. Int. Ed.* **2021**, *60* (18), 10095–10102. DOI: 10.1002/anie.202101158.
(47) Poncet, M.; Benchohra, A.; Jiménez, J.-R.; Piguet, C. Chiral Chromium(III) Complexes as Promising Candidates for Circularly Polarized Luminescence. *ChemPhotoChem* **2021**, *5* (10), 880–892. DOI: 10.1002/cptc.202100146.
(48) Cheng, Y.; He, J.; Zou, W.; Chang, X.; Yang, Q.; Lu, W. Circularly polarized near-infrared phosphorescence of chiral chromium(III) complexes. *Chem. Commun.* **2023**, *59* (13), 1781–1784. DOI: 10.1039/D2CC06548G.
(49) Dorn, M.; Kalmbach, J.; Boden, P.; Päpcke, A.; Gómez, S.; Förster, C.; Kuczelinis, F.; Carrella, L. M.; Büldt, L. A.; Bings, N. H.; Rentschler, E.; Lochbrunner, S.; González, L.; Gerhards, M.; Seitz, M.; Heinze, K. A Vanadium(III) Complex with Blue and NIR-II Spin-Flip Luminescence in Solution. *J. Am. Chem. Soc.* **2020**, *142* (17), 7947–7955. DOI: 10.1021/jacs.0c02122.
(50) Dorn, M.; Kalmbach, J.; Boden, P.; Kruse, A.; Dab, C.; Reber, C.; Niedner-Schatteburg, G.; Lochbrunner, S.; Gerhards, M.; Seitz, M.; Heinze, K. Ultrafast and long-time excited state kinetics of an NIR-emissive vanadium(III) complex I: synthesis, spectroscopy and static quantum chemistry. *Chem. Sci.* **2021**, *12* (32), 10780–10790. DOI: 10.1039/d1sc02137k.
(51) Zobel, J. P.; Knoll, T.; González, L. Ultrafast and long-time excited state kinetics of an NIR-emissive vanadium(III) complex II. Elucidating triplet-to-singlet excited-state dynamics. *Chem. Sci.* **2021**, *12* (32), 10791–10801. DOI: 10.1039/d1sc02149d.
(52) Harris, J. P.; Reber, C.; Colmer, H. E.; Jackson, T. A.; Forshaw, A. P.; Smith, J. M.; Kinney, R. A.; Telser, J. Near-infrared $^2E_g \rightarrow {}^4A_{2g}$ and visible LMCT luminescence from a molecular bis-(tris(carbene)borate) manganese(IV) complex. *Can. J. Chem.* **2017**, *95* (5), 547–552. DOI: 10.1139/cjc-2016-0607.
(53) Jiménez, J.-R.; Doistau, B.; Poncet, M.; Piguet, C. Heteroleptic trivalent chromium in coordination chemistry: Novel building blocks for addressing old challenges in multimetallic luminescent complexes. *Coord. Chem. Rev.* **2021**, *434*, 213750. DOI: 10.1016/j.ccr.2020.213750.
(54) Forster, L. S. The photophysics of chromium(III) complexes. *Chem. Rev.* **1990**, *90* (2), 331–353. DOI: 10.1021/cr00100a001.
(55) Forster, L. S. Thermal relaxation in excited electronic states of d^3 and d^6 metal complexes. *Coord. Chem. Rev.* **2002**, *227* (1), 59–92. DOI: 10.1016/S0010-8545(01)00458-1.
(56) Kirk, A. D. Photochemistry and Photophysics of Chromium(III) Complexes. *Chem. Rev.* **1999**, *99* (6), 1607–1640. DOI: 10.1021/cr960111+.

(57) Kirk, A. D.; Porter, G. B. Luminescence of chromium(III) complexes. *J. Phys. Chem.* **1980**, *84* (8), 887–891. DOI: 10.1021/j100445a020.
(58) Cornioley-Deuschel, C.; Zelewsky, A. von. Stability of d3 diimine complexes: molybdenum(III) vs. chromium(III). *Inorg. Chem.* **1987**, *26* (6), 962–963. DOI: 10.1021/ic00253a040.
(59) Young, C. G. Molybdenum. In *Comprehensive coordination chemistry II*:*From biology to nanotechnology*; McCleverty, J. A., Meyer, T. J., Eds.; Elsevier, 2004; pp 415–527. DOI: 10.1016/B0-08-043748-6/03033-4.
(60) Wang, M.; Weyhermüller, T.; England, J.; Wieghardt, K. Molecular and electronic structures of six-coordinate "low-valent" $[M(^{Me}bpy)_3]^0$ (M = Ti, V, Cr, Mo) and $[M(tpy)_2]^0$ (M = Ti, V, Cr), and seven-coordinate $[MoF(^{Me}bpy)_3](PF_6)$ and $[MX(tpy)_2](PF_6)$ (M = Mo, X = Cl and M = W, X = F). *Inorg. Chem.* **2013**, *52* (21), 12763–12776. DOI: 10.1021/ic402037e.
(61) Beauvais, L. G.; Long, J. R. Cyanide-limited complexation of molybdenum(III): synthesis of octahedral $[Mo(CN)_6]^{3-}$ and cyano-bridged $[Mo_2CN_{11}]^{5-}$. *J. Am. Chem. Soc.* **2002**, *124* (10), 2110–2111. DOI: 10.1021/ja0175901.
(62) Gowda, A. S.; Petersen, J. L.; Milsmann, C. Redox Chemistry of Bis(pyrrolyl)pyridine Chromium and Molybdenum Complexes: An Experimental and Density Functional Theoretical Study. *Inorg. Chem.* **2018**, *57* (4), 1919–1934. DOI: 10.1021/acs.inorgchem.7b02809.
(63) Scarborough, C. C.; Lancaster, K. M.; DeBeer, S.; Weyhermüller, T.; Sproules, S.; Wieghardt, K. Experimental fingerprints for redox-active terpyridine in $[Cr(tpy)_2(PF_6)]^n$ (n = 3-0), and the remarkable electronic structure of $[Cr(tpy)_2]^-$. *Inorg. Chem.* **2012**, *51* (6), 3718–3732. DOI: 10.1021/ic2027219.
(64) Helland, S. D.; Chang, A. S.; Lee, K. W.; Hutchison, P. S.; Brennessel, W. W.; Eckenhoff, W. T. Synthesis and Characterization of Strongly Solvatochromic Molybdenum(III) Complexes. *Inorg. Chem.* **2020**, *59* (1), 705–716. DOI: 10.1021/acs.inorgchem.9b02955.
(65) Hughes, D. L.; Lowe, D. J.; Mohammed, M. Y.; Pickett, C. J.; Pinhal, N. M. Determination of structural features of electrogenerated trans-$[MoCl(NMe)(Ph_2PCH_2CH_2PPh_2)_2]^{2+}$ by multinuclear electron paramagnetic resonance and electron nuclear double resonance spectroscopy and comparison of interatomic distances with those measured by X-ray analysis of the parent monocation. *J. Chem. Soc., Dalton Trans.* **1990** (7), 2021. DOI: 10.1039/DT9900002021.
(66) Maia, L. B.; Moura, I.; Moura, J. J. EPR Spectroscopy on Mononuclear Molybdenum-Containing Enzymes. In *Future Directions in Metalloprotein and Metalloenzyme Research*; Hanson, G., Berliner, L., Eds.; Biological Magnetic Resonance; Springer International Publishing, 2017; pp 55–101. DOI: 10.1007/978-3-319-59100-1_4.
(67) Dhawan, I. K.; Bruck, M. A.; Schilling, B.; Grittini, C.; Enemark, J. H. Mononuclear and Binuclear Molybdenum Complexes of the Tris(3,5-dimethyl-1-pyrazolyl)methane Ligand. *Inorg. Chem.* **1995**, *34* (14), 3801–3808. DOI: 10.1021/ic00118a030.
(68) Krzystek, J.; Ozarowski, A.; Telser, J. Multi-frequency, high-field EPR as a powerful tool to accurately determine zero-field splitting in high-spin transition metal coordination complexes. *Coord. Chem. Rev.* **2006**, *250* (17-18), 2308–2324. DOI: 10.1016/j.ccr.2006.03.016.
(69) Maverick, A. W.; Yao, Q.; Mohammed, A. K.; Henderson, L. J. Photochemistry and Redox Catalysis Using Rhenium and Molybdenum Complexes. In *Photosensitive Metal-*

Organic Systems; Kutal, C., Serpone, N., Eds.; American Chemical Society, 1993; pp 131–146. DOI: 10.1021/ba-1993-0238.ch007.
(70) Mohammed, A. K.; Isovitsch, R. A.; Maverick, A. W. Solution Photophysics, One-Electron Photooxidation, and Photoinitiated Two-Electron Oxidation of Molybdenum(III) Complexes. *Inorg. Chem.* **1998**, *37* (11), 2779–2785. DOI: 10.1021/ic970955r.
(71) Schläfer, H.; Gausmann, H.; Witzke, H. Phosphorescence of molybdenum(III) complexes. *J. Mol. Spectrosc.* **1966**, *21* (1-4), 125–129. DOI: 10.1016/0022-2852(66)90131-7.
(72) Yao, Q.; Maverick, A. W. Near-infrared luminescence of octahedral molybdenum(III) and rhenium(IV) complexes in solution. *Inorg. Chem.* **1988**, *27* (10), 1669–1670. DOI: 10.1021/ic00283a001.
(73) Lever, A. B. P. *Inorganic electronic spectroscopy*, 1st Ed.; Elsevier, 1968.
(74) Dunn, T. M. Spin-orbit coupling in the first and second transition series. *Trans. Faraday Soc.* **1961**, *57*, 1441. DOI: 10.1039/TF9615701441.
(75) Bünzli, J.-C. G.; Eliseeva, S. V. Lanthanide NIR luminescence for telecommunications, bioanalyses and solar energy conversion. *J. Rare Earths* **2010**, *28* (6), 824–842. DOI: 10.1016/S1002-0721(09)60208-8.
(76) Bünzli, J.-C. G. Lanthanide light for biology and medical diagnosis. *J. Lumin.* **2016**, *170*, 866–878. DOI: 10.1016/j.jlumin.2015.07.033.
(77) Kitzmann, W.; Hunger, D.; Reponen, A.-P.; Förster, C.; Schoch, R.; Bauer, M.; Feldmann, S.; van Slageren, J.; Heinze, K. Electronic Structure and Excited State Dynamics of the NIR-II Emissive Molybdenum(III) Analog to the Molecular Ruby. *chemRxiv (Inorganic Chemistry)*, submitted 2023-07-03**.** DOI: 10.26434/chemrxiv-2023-pm760 (accessed 2023-08-18).
(78) Zeng, D.; Hampden-Smith, M. J. High yield routes to molybdenum(III) compounds by diphenylsilane and tin(II) chloride reduction of molybdenum(V) and molybdenum(IV) chlorides. *Polyhedron* **1992**, *11* (20), 2585–2589.
(79) Poli, R.; Krueger, S. T.; Mattamana, S. P. Monomeric Tetrahydrofuran-Stabilized Molybdenum(III) Halides. *Inorg. Synth.* **1998**, *32*, 198–203. DOI: 10.1002/9780470132630.ch33.
(80) Breivogel, A.; Forster, C.; Heinze, K. A heteroleptic bis(tridentate)ruthenium(II) polypyridine complex with improved photophysical properties and integrated functionalizability. *Inorg. Chem.* **2010**, *49* (15), 7052–7056. DOI: 10.1021/ic1007236.
(81) Dorn, M.; Hunger, D.; Förster, C.; Naumann, R.; van Slageren, J.; Heinze, K. Towards Luminescent Vanadium(II) Complexes with Slow Magnetic Relaxation and Quantum Coherence. *Chem. Eur. J.* **2023**, *29* (9), e202202898. DOI: 10.1002/chem.202202898.
(82) Förster, C.; Gorelik, T. E.; Kolb, U.; Ksenofontov, V.; Heinze, K. Crystalline Non-Equilibrium Phase of a Cobalt(II) Complex with Tridentate Ligands. *Chem. Ber.* **2015**, *2015* (6), 920–924. DOI: 10.1002/ejic.201403200.
(83) Förster, C.; Mack, K.; Carrella, L. M.; Ksenofontov, V.; Rentschler, E.; Heinze, K. Coordination of expanded terpyridine ligands to cobalt. *Polyhedron* **2013**, *52*, 576–581. DOI: 10.1016/j.poly.2012.08.008.
(84) Herrmann, S.; Margraf, J. T.; Clark, T.; Streb, C. Thermochromic and solvatochromic properties of Lindqvist polyoxometalates. *Chem. Commun.* **2015**, *51* (71), 13702–13705. DOI: 10.1039/C5CC05730B.

(85) Jiménez, J.-R.; Doistau, B.; Besnard, C.; Piguet, C. Versatile heteroleptic bis-terdentate Cr(III) chromophores displaying room temperature millisecond excited state lifetimes. *Chem. Commun.* **2018**, *54* (94), 13228–13231. DOI: 10.1039/c8cc07671e.
(86) Zare, D.; Doistau, B.; Nozary, H.; Besnard, C.; Guénée, L.; Suffren, Y.; Pelé, A.-L.; Hauser, A.; Piguet, C. CrIII as an alternative to RuII in metallo-supramolecular chemistry. *Dalton. Trans.* **2017**, *46* (28), 8992–9009. DOI: 10.1039/c7dt01747b.
(87) Gatehouse, B. M.; Nunn, E. K. The crystal and molecular structure of di-μ-oxo-bis[2,2'-bipyridyloxohypophosphitomolybdenum(V)]. *Acta Crystallogr. B Struct. Sci.* **1976**, *32* (9), 2627–2630. DOI: 10.1107/S0567740876008388.
(88) Zhou, Z.-H.; Deng, Y.-F.; Cao, Z.-X.; Zhang, R.-H.; Chow, Y. L. Dimeric dioxomolybdenum(VI) and oxomolybdenum(V) complexes with citrate at very low pH and neutral conditions. *Inorg. Chem.* **2005**, *44* (20), 6912–6914. DOI: 10.1021/ic048330y.
(89) Dinoi, C.; Guedes da Silva, M. F. C.; Alegria, E. C. B. A.; Smoleński, P.; Martins, L. M. D. R. S.; Poli, R.; Pombeiro, A. J. L. Molybdenum Complexes Bearing the Tris(1-pyrazolyl)methanesulfonate Ligand: Synthesis, Characterization and Electrochemical Behaviour. *Eur. J. Inorg. Chem.* **2010**, *2010* (16), 2415–2424. DOI: 10.1002/ejic.201000018.
(90) Bridgeman, A. J.; Cavigliasso, G. Structure and bonding in $[M_6O_{19}]^{n-}$ isopolyanions. *Inorg. Chem.* **2002**, *41* (7), 1761–1770. DOI: 10.1021/ic011086f.
(91) Lueken, H. *Magnetochemie*:*Eine Einführung in Theorie und Anwendung*; Teubner Studienbücher Chemie; Vieweg+Teubner Verlag, 1999. DOI: 10.1007/978-3-322-80118-0.
(92) Bamberger, H.; Albold, U.; Dubnická Midlíková, J.; Su, C.-Y.; Deibel, N.; Hunger, D.; Hallmen, P. P.; Neugebauer, P.; Beerhues, J.; Demeshko, S.; Meyer, F.; Sarkar, B.; van Slageren, J. Iron(II), Cobalt(II), and Nickel(II) Complexes of Bis(sulfonamido)benzenes: Redox Properties, Large Zero-Field Splittings, and Single-Ion Magnets. *Inorg. Chem.* **2021**, *60* (5), 2953–2963. DOI: 10.1021/acs.inorgchem.0c02949.
(93) Stuart, R.; Marshall, W. Direct Exchange in Ferromagnets. *Phys. Rev.* **1960**, *120* (2), 353–357. DOI: 10.1103/PhysRev.120.353.
(94) Bose, M.; Moula, G.; Sarkar, S. A cyanide-bridged molybdenum bis(maleonitriledithiolate) square. *Inorg. Chem.* **2014**, *53* (1), 6–8. DOI: 10.1021/ic402160h.
(95) Akagi, S.; Fujii, S.; Kitamura, N. Zero-Magnetic-Field Splitting in the Excited Triplet States of Octahedral Hexanuclear Molybdenum(II) Clusters: $\{Mo_6X_8\}Y_6^{2-}$ (X, Y = Cl, Br, I). *J. Phys. Chem. A* **2018**, *122* (46), 9014–9024. DOI: 10.1021/acs.jpca.8b09339.
(96) Averill, B. A.; Orme-Johnson, W. H. Electron paramagnetic resonance spectra of molybdenum(III) complexes: direct observation of molybdenum-95 hyperfine interaction and implications for molybdoenzymes. *Inorg. Chem.* **1980**, *19* (6), 1702–1705. DOI: 10.1021/ic50208a054.
(97) Jarrett, H. S. Paramagnetic Resonance in Trivalent Transition Metal Complexes. *J. Chem. Phys.* **1957**, *27* (6), 1298–1304. DOI: 10.1063/1.1743995.
(98) Gregson, A. K.; Anker, M. The Low-Temperature Magnetic Properties of Tris(acetylacetonato)molybdenum(III). *Aust. J. Chem.* **1979**, *32* (3), 503. DOI: 10.1071/CH9790503.
(99) Shores, M. P.; Sokol, J. J.; Long, J. R. Nickel(II)-molybdenum(III)-cyanide clusters: synthesis and magnetic behavior of species incorporating $(Me_3tacn)Mo(CN)_3$. *J. Am. Chem. Soc.* **2002**, *124* (10), 2279–2292. DOI: 10.1021/ja011645h.
(100) Mousavi, M.; Béreau, V.; Desplanches, C.; Duhayon, C.; Sutter, J.-P. Substantial exchange coupling for {Mo-NCS-M} combination: illustration for 1-D

{Mo(NCS)$_6$}{NiL}$_2$(NCS)$_n$. *Chem. Commun.* **2010**, *46* (40), 7519–7521. DOI: 10.1039/C0CC02498H.
(101) Plasser, F. TheoDORE: A toolbox for a detailed and automated analysis of electronic excited state computations. *J. Chem. Phys.* **2020**, *152* (8), 84108. DOI: 10.1063/1.5143076.
(102) Treadway, J. A.; Strouse, G. F.; Ruminski, R. R.; Meyer, T. J. Long-lived near-infrared MLCT emitters. *Inorg. Chem.* **2001**, *40* (18), 4508–4509. DOI: 10.1021/ic010660k.
(103) Xiang, H.; Cheng, J.; Ma, X.; Zhou, X.; Chruma, J. J. Near-infrared phosphorescence: materials and applications. *Chem. Soc. Rev.* **2013**, *42* (14), 6128–6185. DOI: 10.1039/C3CS60029G.
(104) Willis, O. G.; Petri, F.; Pescitelli, G.; Pucci, A.; Cavalli, E.; Mandoli, A.; Zinna, F.; Di Bari, L. Efficient 1400-1600 nm Circularly Polarized Luminescence from a Tuned Chiral Erbium Complex. *Angew. Chem. Int. Ed.* **2022**, *61* (34), e202208326. DOI: 10.1002/anie.202208326.
(105) Yang, Y.; Tu, D.; Zhang, Y.; Zhang, P.; Chen, X. Recent advances in design of lanthanide-containing NIR-II luminescent nanoprobes. *iScience* **2021**, *24* (2), 102062. DOI: 10.1016/j.isci.2021.102062.
(106) Beć, K. B.; Karczmit, D.; Kwaśniewicz, M.; Ozaki, Y.; Czarnecki, M. A. Overtones of νC≡N Vibration as a Probe of Structure of Liquid CH_3CN, CD_3CN, and CCl_3CN: Combined Infrared, Near-Infrared, and Raman Spectroscopic Studies with Anharmonic Density Functional Theory Calculations. *J. Phys. Chem. A* **2019**, *123* (20), 4431–4442. DOI: 10.1021/acs.jpca.9b02170.
(107) Bulmer, J. T.; Shurvell, H. F. Factor analysis as a complement to band resolution techniques. II. Pseudoisobestic point in the chloroform-d-dibutyl ether system. *J. Phys. Chem.* **1973**, *77* (17), 2085–2090. DOI: 10.1021/j100636a011.
(108) Jones, R. W.; Auty, A. J.; Wu, G.; Persson, P.; Appleby, M. V.; Chekulaev, D.; Rice, C. R.; Weinstein, J. A.; Elliott, P. I. P.; Scattergood, P. A. Direct Determination of the Rate of Intersystem Crossing in a Near-IR Luminescent Cr(III) Triazolyl Complex. *J. Am. Chem. Soc.* **2023**, *145* (22), 12081–12092. DOI: 10.1021/jacs.3c01543.
(109) Shafikov, M. Z.; Zaytsev, A. V.; Kozhevnikov, V. N. Halide-Enhanced Spin-Orbit Coupling and the Phosphorescence Rate in Ir(III) Complexes. *Inorg. Chem.* **2021**, *60* (2), 642–650. DOI: 10.1021/acs.inorgchem.0c02469.
(110) Yersin, H.; Czerwieniec, R.; Monkowius, U.; Ramazanov, R.; Valiev, R.; Shafikov, M. Z.; Kwok, W.-M.; Ma, C. Intersystem crossing, phosphorescence, and spin-orbit coupling. Two contrasting Cu(I)-TADF dimers investigated by milli- to micro-second phosphorescence, femto-second fluorescence, and theoretical calculations. *Coord. Chem. Rev.* **2023**, *478*, 214975. DOI: 10.1016/j.ccr.2022.214975.
(111) Kitzmann, W. R.; Heinze, K. Charge-Transfer and Spin-Flip States: Thriving as Complements. *Angew. Chem. Int. Ed.* **2023**, *62* (15), e202213207. DOI: 10.1002/anie.202213207.
(112) Marian, C. M. Spin-orbit coupling and intersystem crossing in molecules. *WIREs Comput. Mol. Sci.* **2012**, *2* (2), 187–203. DOI: 10.1002/wcms.83.
(113) Perkovic, M. W.; Heeg, M. J.; Endicott, J. F. Stereochemical perturbations of the relaxation behavior of (^{2}E)chromium(III). Ground-state x-ray crystal structure, photophysics, and molecular mechanics simulations of the quasi-cage complex [4,4',4"-ethylidynetris(3-azabutan-1-amine)]chromium tribromide. *Inorg. Chem.* **1991**, *30* (16), 3140–3147. DOI: 10.1021/ic00016a009.

(114) Otto, S.; Förster, C.; Wang, C.; Resch-Genger, U.; Heinze, K. A Strongly Luminescent Chromium(III) Complex Acid. *Chem. Eur. J.* **2018**, *24* (48), 12555–12563. DOI: 10.1002/chem.201802797.
(115) Treiling, S.; Wang, C.; Förster, C.; Reichenauer, F.; Kalmbach, J.; Boden, P.; Harris, J. P.; Carrella, L. M.; Rentschler, E.; Resch-Genger, U.; Reber, C.; Seitz, M.; Gerhards, M.; Heinze, K. Luminescence and Light-Driven Energy and Electron Transfer from an Exceptionally Long-Lived Excited State of a Non-Innocent Chromium(III) Complex. *Angew. Chem. Int. Ed.* **2019**, *58* (50), 18075–18085. DOI: 10.1002/anie.201909325.

For Table of Contents Only

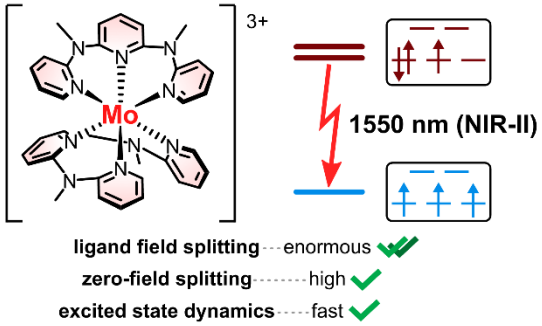

Luminescent chromium(III) complexes have been studied in great detail during the past decades. In contrast, only 10 emissive molybdenum(III) complexes have been reported so far. Here, we present two heteroleptic and one homoleptic molybdenum(III) complexes that show weak spin-flip emission in the NIR-II peaking up to 1550 nm. We lay out the reasons for this intriguing behavior based on EPR and fs-transient absorption spectroscopy supplemented with multi-reference calculations and suggest design strategies for the future.